

First-principles study of electronic, elastic and optical properties of $Zn_{1-x}Mg_xTe$ ternary alloys using modified Becke–Johnson potential

M. RASHID^{a*}, G. S. ABO^b, S. A. AHMAD^c, M. IMRAN^d, M. A. SAEED^e, F. HUSSAIN^d, N. A. NOOR^f

^aDepartment of Physics, COMSATS Institute of Information Technology (CIIT), 44000 Islamabad, Pakistan

^bDepartment of Electrical and Computer Engineering and MINT Center, The University of Alabama, Tuscaloosa, AL 35487, USA

^cDepartment of Physics Simulation Lab, the Islamia University of Bahawalpur, 63100, Pakistan

^dDepartment of Physics, Bahauddin Zakariya University, Multan, Pakistan, 60800

^eDepartment of Physics, Faculty of Science, Universiti Teknologi Malaysia, Skudai-81310, Johor, Malaysia

^fDepartment of Physics, University of the Punjab, Quaid-e-Azam Campus, 54590 Lahore, Pakistan

The electronic, elastic and optical properties of binary ZnTe, MgTe and their ternary $Zn_{1-x}Mg_xTe$ alloys ($0 \leq x \leq 1$) in zinc blende phase have been studied using the modified Becke–Johnson (mBJ) potential within the framework of density functional theory (DFT). We employed the special quasi-random structures (SQS) method. Wu–Cohen (WC), PBE for solids (PBEsol) and Perdew–Burke–Ernzerhof (PBE) generalized gradient approximations (GGA) were also used to calculate the exchange–correlation and electronic band gap energies. The calculated band structures show that the crystal is a semiconductor with a direct band gap, and the contribution of Zn-3d and Te-5p are prominent in the density of states (DOS). We have predicted the basic optical properties: dielectric function, refractive index and optical reflectivity. The calculated binary alloy results are in agreement with existing experimental and theoretical values.

(Received June 2, 2014; accepted May 7, 2015)

Keywords: Ab initio calculations, Electronic structure, Optical properties, Elastic properties

1. Introduction

The II–VI semiconductors have been of interest because of their wide band gap characteristic and their potential applications for optoelectronic devices [1]. The ternary and quaternary alloys of II–VI semiconductors have large optical gaps and feasibility of whole spectral range from infrared (IR) to ultraviolet (UV) for optoelectronic devices [2]. These materials are used to construct X-ray and γ -ray detectors [3]. Due to their large and direct gap character, ZnTe based semiconductors have been suggested as new materials for a wide range of optoelectronics. ZnTe and MgTe are II–VI semiconductors and have a cubic phase, called the zinc blende (ZB) structure [4]. Mixed crystals of Mg chalcogenide compounds have attracted considerable attention due to successful fabrication of blue and blue-green injection laser diodes by molecular beam epitaxy (MBE) [5].

$Zn_{1-x}Mg_xSe$ has been studied experimentally, $Zn_{1-x}Mg_xTe$ mixed ternary alloys are suitable materials for a cladding layer, and a transparent ZnTe substrate established pure green light emitting diode (LED) [6]. The experimental description for P-doped $Zn_{1-x}Mg_xTe$ single crystals of composition, transmission and reflection spectra, photoluminescence spectra and electrical properties has been a significant step towards realizing ZnTe based LED with high performance [7]. The preparation and optical properties measurement of ZnTe based single crystal for optoelectronic devices is described in [8]. On the other hand, it is possible to develop epitaxial

layers of $Zn_{1-x}Mg_xTe$ over the full composition range, including zinc blende MgTe and also on their ternary compounds using MBE [9].

In so far as we know, there is no systematic theoretical study on the optical properties of $Zn_{1-x}Mg_xTe$ mixed crystals in related literature. To attain more accurate theoretical results for $Zn_{1-x}Mg_xTe$ in zinc blende phase, modified Becke–Johnson (mBJ) potential [10] was used, which gives band gap values closer to experimental data than LDA or GGA. The mBJ potential has been successfully used to calculate precisely the band gap for a wide range of different materials [11]. This potential depends on the density of kinetic energy and defines the excited states of insulators and semiconductors by producing an accurate shape of the exact exchange potential [12]. In the present paper, we make use of ‘special quasi-random structure’ (SQS) approach as compared to an earlier study where high symmetry ordered supercells have been used for the obtaining electronic structure of the $Zn_{1-x}Mg_xTe$ alloys. In addition to obtaining the structural, electronic and optical properties, we also compare our obtained results using SQS approach with Ref. [13] to establish that the former provides a much improved electronic structures approximation as already justified by Zunger and co-workers [14].

2. Method of calculation

In order to study the electronic and optical properties of $Zn_{1-x}Mg_xTe$ at $x = 0.0, 0.25, 0.50, 0.75,$ and 1.0 in zinc

blende phase, the full-potential linear augmented plane waves plus local orbitals (FP-LAPW+lo) method was used to solve the Kohn–Sham equation within the density functional theory (DFT) [15] formulation as employed in WIEN2k [16]. The mBJ potential for the exchange–correlation potential [10] was used to calculate electronic and optical properties. The special quasi-random structures (SQS) approach of Zunger et al. [14] was used to replicate the randomness of the alloys around a given site for the first few shells. This approach is effective in reducing the size of the supercells for calculating many properties of random alloys. It is also realistically sufficient to describe the physical properties of many alloys that are not affected by the errors associated with using the concept of periodicity beyond the first few shells. Inside the non-overlapping spheres of radius R_{MT} around every atom, spherical harmonic expansion is used, and the plane wave basis set was chosen in the remaining space of the cell. The radius of muffin-tin (R_{MT}) spheres values for Zn, Mg and Te atoms were taken to be 2.2, 2.15 and 2.3 a.u., respectively. The plane wave cut off parameters were $R_{MT} \times K_{max} = 7$ (where K_{max} is the largest wave vector of the basis set) and $G_{max} = 12$ (Ryd)^{1/2}. We used 500 k -points in these calculations to reduce the wedge of the Brillouin zone for $x = 0.25, 0.50$ and 0.75 , respectively, to calculate the structural and electronic properties. While for the calculations of the optical properties of binary and their ternary alloys, a dense mesh of uniformly distributed $10 \times 10 \times 5$ k -points are used in the first Brillouin zone. When the total energy convergence is less than 10^{-5} Ry, the self-consistent calculation is considered to be stable. The orbitals of Zn ($3d^{10} 4s^2$), Mg ($1s^2 2s^2 2p^6 3s^2$) and Te ($4d^{10} 5s^2 5p^4$) are treated as valence electrons. Perdew–Burke–Ernzerhof (PBE), Wu and Cohen (WC), PBE for solids (PBEsol) generalized gradient approximation (GGA) schemes were also used for finding the band gaps. The optical properties were computed using the optical properties module within WIEN2k [17].

3. Results and discussion

3.1. Electronic Properties

In structural optimization, theoretical modeling of the binary ZnTe and MgTe compounds and their $Zn_{1-x}Mg_xTe$ alloys at selected compositions $x = 0.25, 0.50$ and 0.75 in ZB phase have been used to compute the structural properties with WC GGA scheme. The SQS approach is applied to get ordered cubic structures in ZB phase at $x = 0.25, 0.50$ and 0.75 . As a result, small supercell periodic structures with simple cubic lattice at the compositions of $x = 0.25$ and 0.75 are obtained with space group P43m, whereas for $x = 0.50$, the ordered structure is a different space group P_{222} in ZB phase. The $2 \times 2 \times 1$ supercells with 32 atoms for the different compositions of $x = 0, 0.25, 0.50, 0.75$ and 1.0 are presented in Fig. 1.

The band gaps of binary ZnTe and MgTe compounds and their ternary $Zn_{1-x}Mg_xTe$ alloys with various compositions at $x = 0.0, 0.25, 0.50, 0.75$, and 1.0 in the ZB phase were calculated with the WC GGA scheme [18] using SQS approach. The band gaps of the binary compounds as well as for their ternary alloys were also calculated using the mBJ potential at the Γ -point at concentrations of $x = 0, 0.25, 0.50, 0.75$, and 1.0 . The calculated band gaps for the binary and their ternary alloys are summarized and compared to other theoretical and experimental results in Table 1. It is obviously seen that the presented band gap (E_g) values from the calculations are in decent agreement with the experimental values. Chung et al. [19] found experimentally that the band gap was quite linear between x of 0 and 0.48, and their linear fit of $E_g = ax + b$ gave $a = 0.8$ and $b = 4.2$. The fit of the mBJ values in Table 1 between $x = 0$ and 0.5 was found to be in fair agreement with $a = 0.92$ and $b = 1.8$. In addition, the band shapes concur well with the previous theoretical works for ZnTe and MgTe.

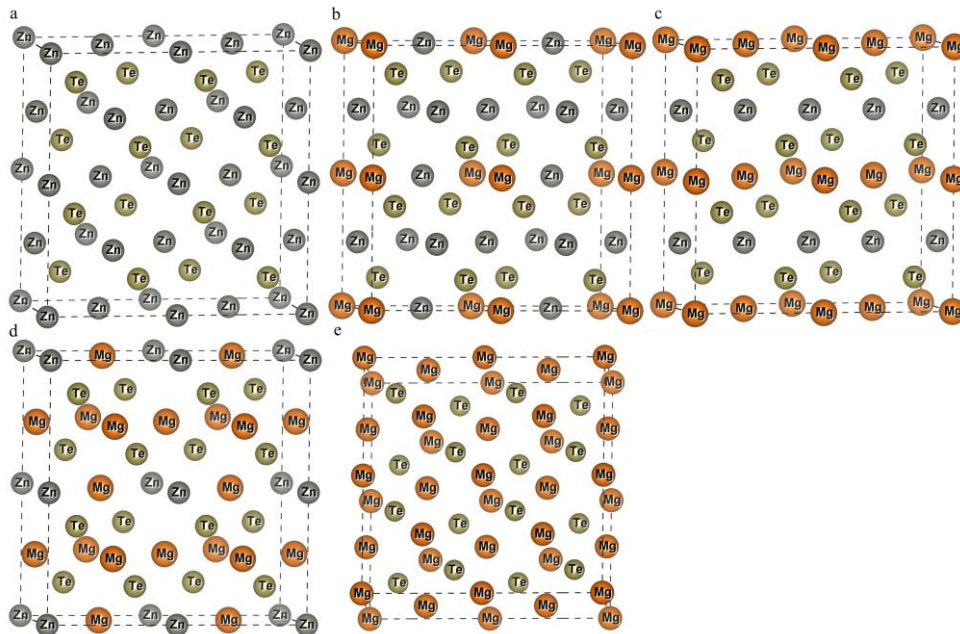


Fig. 1. Crystal structure of $Zn_{1-x}Mg_xTe$ alloy at $x =$ (a) 0, (b) 0.25, (c) 0.50, (d) 0.75 and (e) 1.0 in zinc blende phase.

Therefore, only the mBJ results are plotted and same patterns were observed for the PBE GGA, WC GGA, and PBEsol GGA. The calculated band structures for the ternary alloys along the higher symmetry directions, R, Γ , M and X in the Brillouin zone using mBJ approach are shown in Fig. 2. The valence band maximum (VBM) is situated at the Γ -point, whereas the conduction band minimum (CBM) is also located at the Γ -point, which results in a direct band gap (Γ - Γ) in all binary and ternary compounds. It is an advantage to have a direct gap as it

makes a vertical optical transition, which can be utilized in photonic and optoelectronic devices [20]. It can be seen from Fig. 2 that the band gaps increase with increase in the concentration of Mg, and similar behavior was observed experimentally [21, 22]. This increase in the energy gap can be accredited to the fact that the conduction bands move away from the Fermi energy (E_F).

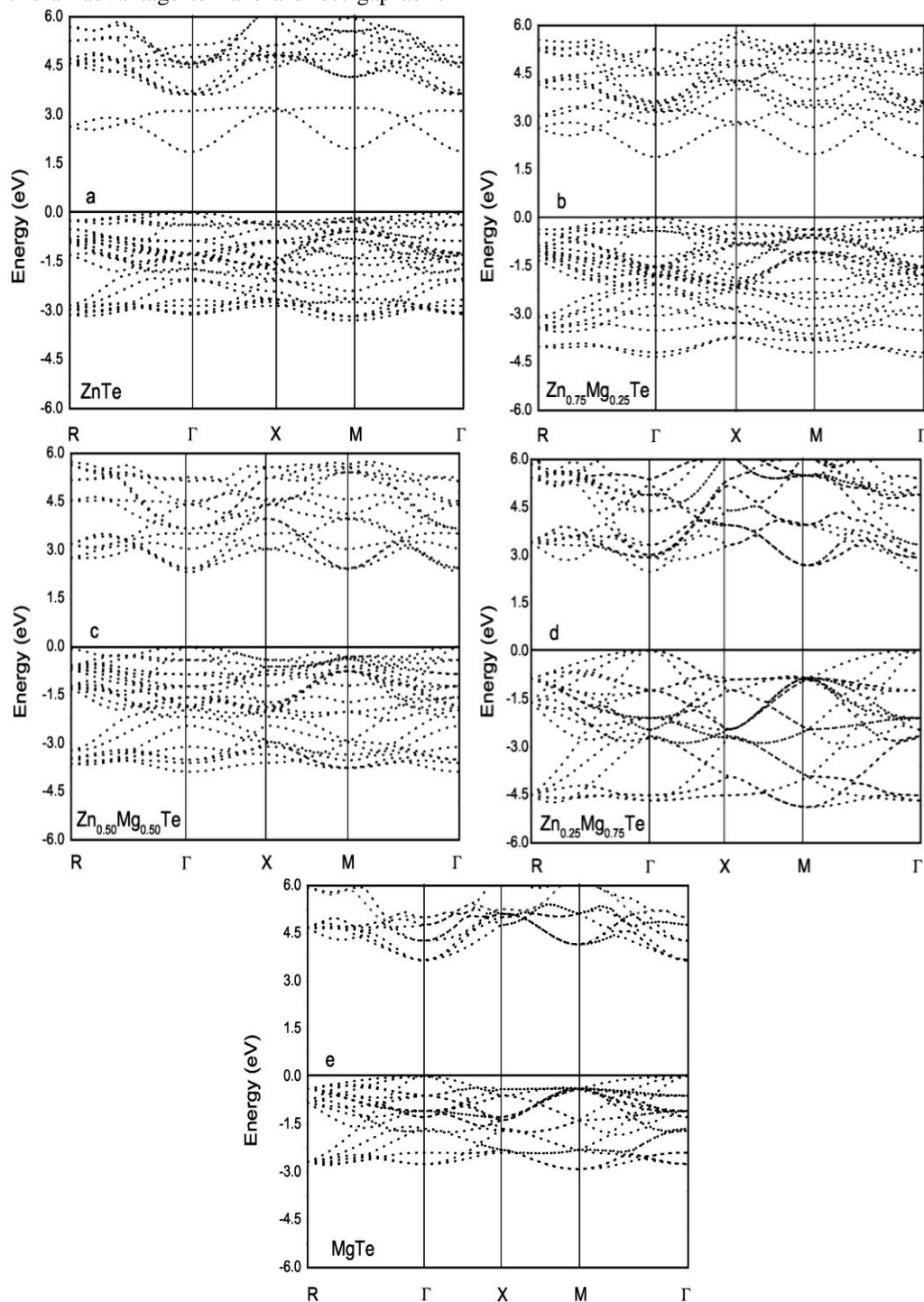


Fig. 2. Band structures of $\text{Zn}_{1-x}\text{Mg}_x\text{Te}$ at various compositions of $x = (a) 0, (b) 0.25, (c) 0.50, (d) 0.75$ and $(e) 1.0$ using mBJ.

Table 1. Calculated band gaps for $Zn_{1-x}Mg_xTe$ at Γ - Γ symmetry points.

Composition	Band gap energy (eV)						
	x	GGA(WC)	GGA(PBEsol)	GGA(PBE)	mBJ	Experimental	Others work
0.00		1.33	1.37	1.46	1.85	2.2 ^[23] , 2.28 ^[24]	2.1 ^[25] , 2.26 ^[26]
0.25		1.46	1.48	1.54	2.01		
0.50		1.61	1.63	1.69	2.31		
0.75		2.01	2.06	2.12	2.73		
1.00		2.61	2.62	2.69	3.55	3.5 ^[27]	2.47 ^[28] , 3.2 ^[29]

With the optimized crystal structure, the total density of states (DOS) and partial DOS using mBJ were calculated as shown in Fig. 3. The character of the band states can be found for these materials by calculating the total and partial DOS. The ZnTe and MgTe compounds both have discrete energy gaps between the valence and the conduction energy bands. Furthermore, there is a large DOS peak arising from the Zn-3d state. As can be

expected, the valence band is dominated by Zn-3d from -6 to -7 eV, while Te-5s states occur from -9.5 to -10.5 eV and Te-5p from -0.2 to -3.6 eV in ternary alloys. The Mg-3s states have a slightly small involvement at -2.4 to -2.9 eV of the valence band for MgTe. For the binary compound of MgTe, the upper part of the conduction band is shaped by a mixture of Mg-3s and Mg-2p states.

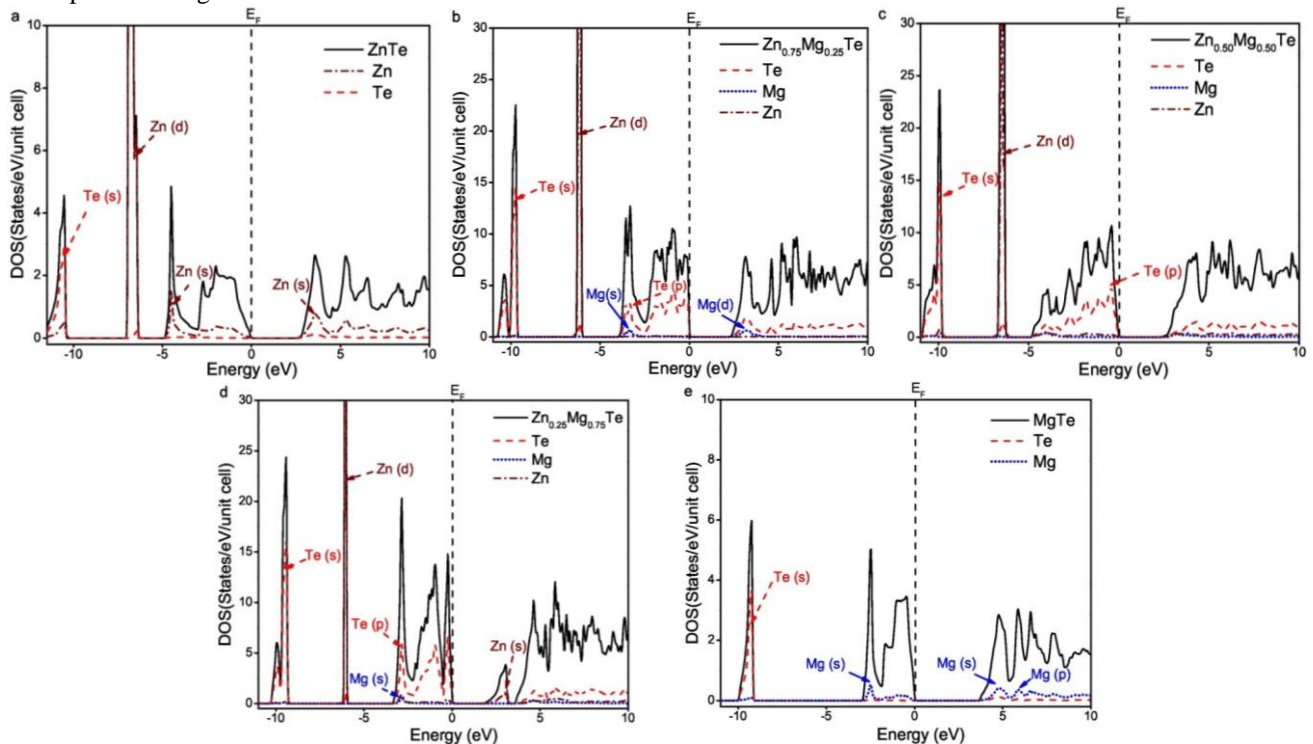


Fig. 3. Total and partial density of states (DOS) using different potentials at $x =$ (a) 0.0, (b) 0.25, (c) 0.50, (d) 0.75, and (e) 1.0 for $Zn_{1-x}Mg_xTe$ alloys.

One of the more apparent ways to investigate the nature of the chemical bonding in a compound is merely to study the charge density. Our mBJ results for the electronic charge density in the (110) plane of binary ZnTe and MgTe compounds and their ternary alloys at $x = 0.25, 0.50,$ and 0.75 are shown in Fig. 4, respectively. The calculated electron charge distribution shows that there is a durable ionic character and strong covalent bonding as can be seen along the Zn-Te bonds in binary ZnTe and their ternary alloys. It can be seen in Fig. 4 that the spreading of

electron density for Te is not symmetric, and the electron densities between Te and Zn change at various compositions. Ionic bonding is perceived in the Mg-Te bond as the concentration of Mg is increased. In other words, the covalent bonding becomes weak and shifts towards ionic bonding, but as a whole, it is partially covalent and ionic in nature [30].

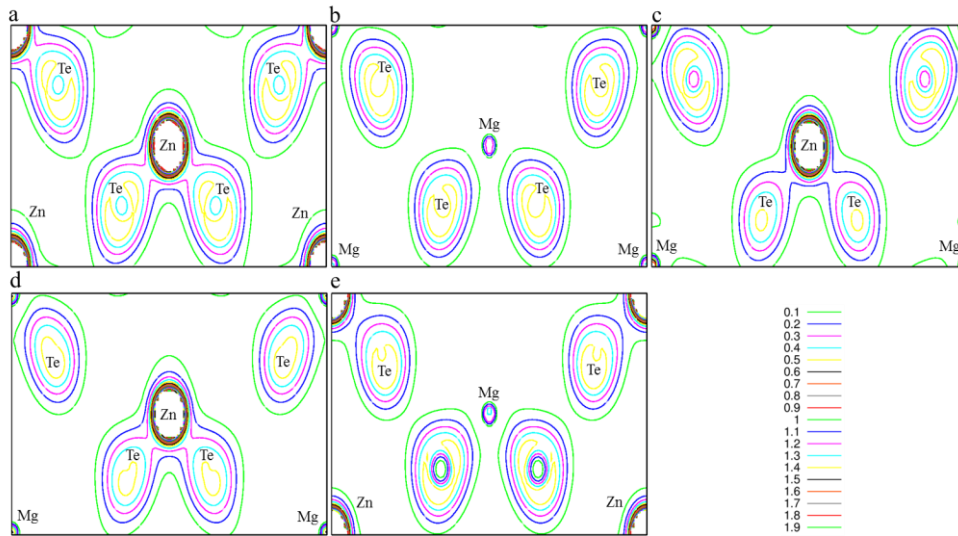


Fig. 4. Calculated contour plots of electronic charge densities in the (110) plane for $\text{Zn}_{1-x}\text{Mg}_x\text{Te}$ at composition x of (a) 0, (b) 1.0, (c) 0.25, (d) 0.50 and (e) 0.75.

3.2. Elastic Properties

The elastic constants of solids give a relation between the mechanical and dynamical behavior of crystals and provide essential information about the nature of the forces operating in solids. In particular, they give the information about the stability and rigorousness of materials. The elastic constants are significant parameters that describe the reaction on applied macroscopic stress. To find the elastic constants of $\text{Zn}_{1-x}\text{Mg}_x\text{Te}$ alloys with cubic structure, first principles calculation was used to compute the components of the stress tensor ε for small strains using the method developed by Charpin and integrated in the WIEN2k [16]. It is well-known that a cubic crystal has only three independent elastic constants, C_{11} , C_{12} and C_{44} . The elastic constants make it possible to determine the bulk modulus and shear modulus.

For cubic crystals, the bulk modulus (B_S) and the shear wave modulus (C_S) are given respectively by [31]:

$$B_S = \frac{C_{11} + 2C_{12}}{3} \quad (1)$$

$$C_S = \frac{C_{11} - C_{12}}{2} \quad (2)$$

The calculated three independent elastic constants C_{11} , C_{12} and C_{44} , bulk modulus B_S and shear modulus C_S for binary and ternary alloys of $\text{Zn}_{1-x}\text{Mg}_x\text{Te}$ at various composition of $x = 0.0, 0.25, 0.50, 0.75$, and 1.0 in ZB phase are given in Table 2. As shown, the calculated results are in fair agreement with available experimental and theoretical data [32, 33].

Table 2. Calculated elastic constants (C_{11} , C_{12} and C_{44}), bulk modulus (B_S) and shear modulus (C_S) in GPa of $\text{Zn}_{1-x}\text{Mg}_x\text{Te}$.

x	C_{11}	C_{12}	C_{44}	B_S	C_S	Reference
0.00	95.10	51.20	60.85	65.80	21.95	Present
	82	42	55	50.9	20	Theory ^[34]
	71.1	40.7	31.3	50.8	-	Experiment ^[35]
0.25	91.47	47.84	51.27	62.38	21.50	Present
0.50	83.29	42.76	45.69	56.27	20.72	Present
0.75	75.36	39.15	42.90	51.22	18.12	Present
1.00	68.43	33.72	40.94	45.29	17.35	Present
	61.2	28.2	48.27	38.7	-	Theory ^[36]

3.3. Optical Properties

The optical properties of matter can be characterized by the dielectric function $\varepsilon(\omega)$, which describes the linear response of the system to an external electromagnetic field with a small wave vector and the absorption properties of the material. The dielectric function is $\varepsilon(\omega) = \varepsilon_1(\omega) + i$

$\varepsilon_2(\omega)$, where $\varepsilon_1(\omega)$ and $\varepsilon_2(\omega)$ are the real and the imaginary parts, respectively. The $\varepsilon_1(\omega)$ and $\varepsilon_2(\omega)$ are calculated using the standard Kramers–Krönig relationship [37]. The real and imaginary parts of the dielectric constant for binary and ternary compounds are calculated at various composition of $x = 0.0, 0.25, 0.50, 0.75$, and 1.0. The plots presented in Fig. 5a-b with energies up to 14 eV are

for $\varepsilon_1(\omega)$ and $\varepsilon_2(\omega)$, respectively, in zinc blende phase. The behavior of $\varepsilon_1(\omega)$ and $\varepsilon_2(\omega)$ are similar for these compounds with some variances in details. The core feature of the $\varepsilon_1(\omega)$ curves is that the main absorbance peak arises at 2.78, 3.16, 3.87, 4.72, and 4.88 eV, respectively, for compositions of x from 0 to 1.0 as shown in Fig. 5a. These peaks decrease due to the interband transition and all become negative at about 6 eV for each composition of x . The dielectric constant, $\varepsilon_1(0)$, is found to be 6.59, 6.38, 5.95, 5.42, and 4.91 for each composition of

$x = 0.0, 0.25, 0.50, 0.75,$ and 1.0 for $\text{Zn}_{1-x}\text{Mg}_x\text{Te}$ and show similar behavior to $\text{Zn}_{1-x}\text{Mg}_x\text{Se}$ [38]. The absorption begins at about 1.91, 2.18, 2.33, 2.35, and 3.56 eV for the imaginary part of the dielectric function at same compositions of x , respectively, as can be seen in Fig. 5b. The main peaks in the imaginary part occur in the range of 3.7 to 6.3 eV. Our calculated dielectric results are in good agreement with those available for binary compounds ZnTe [34] and MgTe [36].

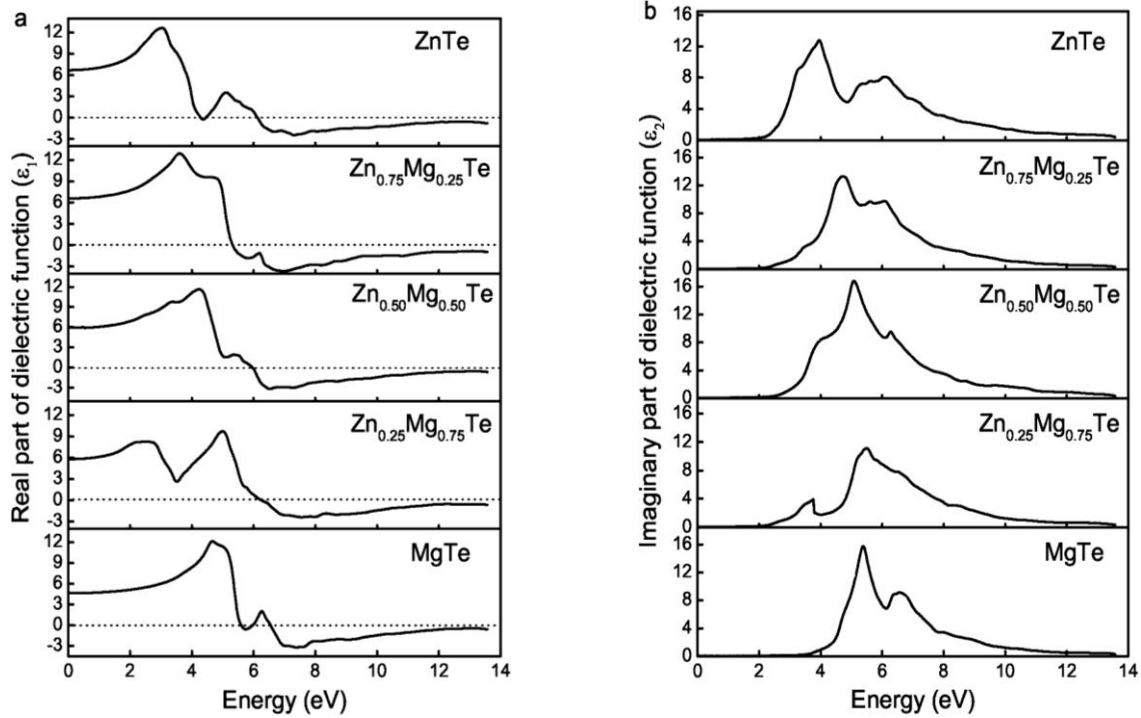


Fig. 5. Dielectric constant for $\text{Zn}_{1-x}\text{Mg}_x\text{Te}$ corresponding to different values of x for (a) $\varepsilon_1(\omega)$ and (b) $\varepsilon_2(\omega)$.

$n(\omega)$ is the real part of the refractive index, which explains how light or radiation propagates through a solid. The relation between the refractive index $n(0)$ and $\varepsilon_1(0)$ is $n(0) = [\varepsilon_1(0)]^{1/2}$. The real and imaginary parts of the dielectric function are used to calculate the reflectivity coefficient $R(\omega)$ as well as the refractive index $n(\omega)$ and extinction coefficient $k(\omega)$.

The awareness of both real and imaginary parts of the dielectric function permits the calculation of important optical functions such as refractive index, extinction coefficient and reflectivity using the following equations [39]:

$$n(\omega) = \frac{1}{\sqrt{2}} \left[\left\{ \varepsilon_1(\omega)^2 + \varepsilon_2(\omega)^2 \right\}^{1/2} + \varepsilon_1(\omega) \right]^{1/2} \quad (3)$$

$$k(\omega) = \frac{1}{\sqrt{2}} \left[\left\{ \varepsilon_1(\omega)^2 + \varepsilon_2(\omega)^2 \right\}^{1/2} - \varepsilon_1(\omega) \right]^{1/2} \quad (4)$$

$$R(\omega) = \frac{(n-1)^2 + k^2}{(n+1)^2 + k^2} \quad (5)$$

The calculated $n(\omega)$, $k(\omega)$ and $R(\omega)$ of $\text{Zn}_{1-x}\text{Mg}_x\text{Te}$ for each composition of x in the energy range from 0 to 14 eV is plotted in Fig. 6. Fig. 6a shows the plots of refractive index $n(\omega)$ for $\text{Zn}_{1-x}\text{Mg}_x\text{Te}$ alloys at concentration $x = 0.0, 0.25, 0.50, 0.75,$ and 1.0 , while Fig. 6b shows that the $k(\omega)$ follows the $\varepsilon_2(\omega)$. The maximum peak moves towards higher energy levels as the concentration of Mg is increased [40]. The reflectivity coefficient $R(\omega)$ depends on $\varepsilon_1(\omega)$ and $\varepsilon_2(\omega)$. The maximum peak of $R(\omega)$ occurs after 13 eV for each concentration as shown in Fig. 6c. It means that maximum reflection appears beyond 13 eV. The calculated values of $n(0)$, $R(0)$ and the optical dielectric constants that have been obtained at various compositions of $x = 0.0, 0.25, 0.50, 0.75,$ and 1.0 are given in Table 3. The values of $n(0)$, for their corresponding zero frequency refractive index, decrease with increasing Mg concentration.

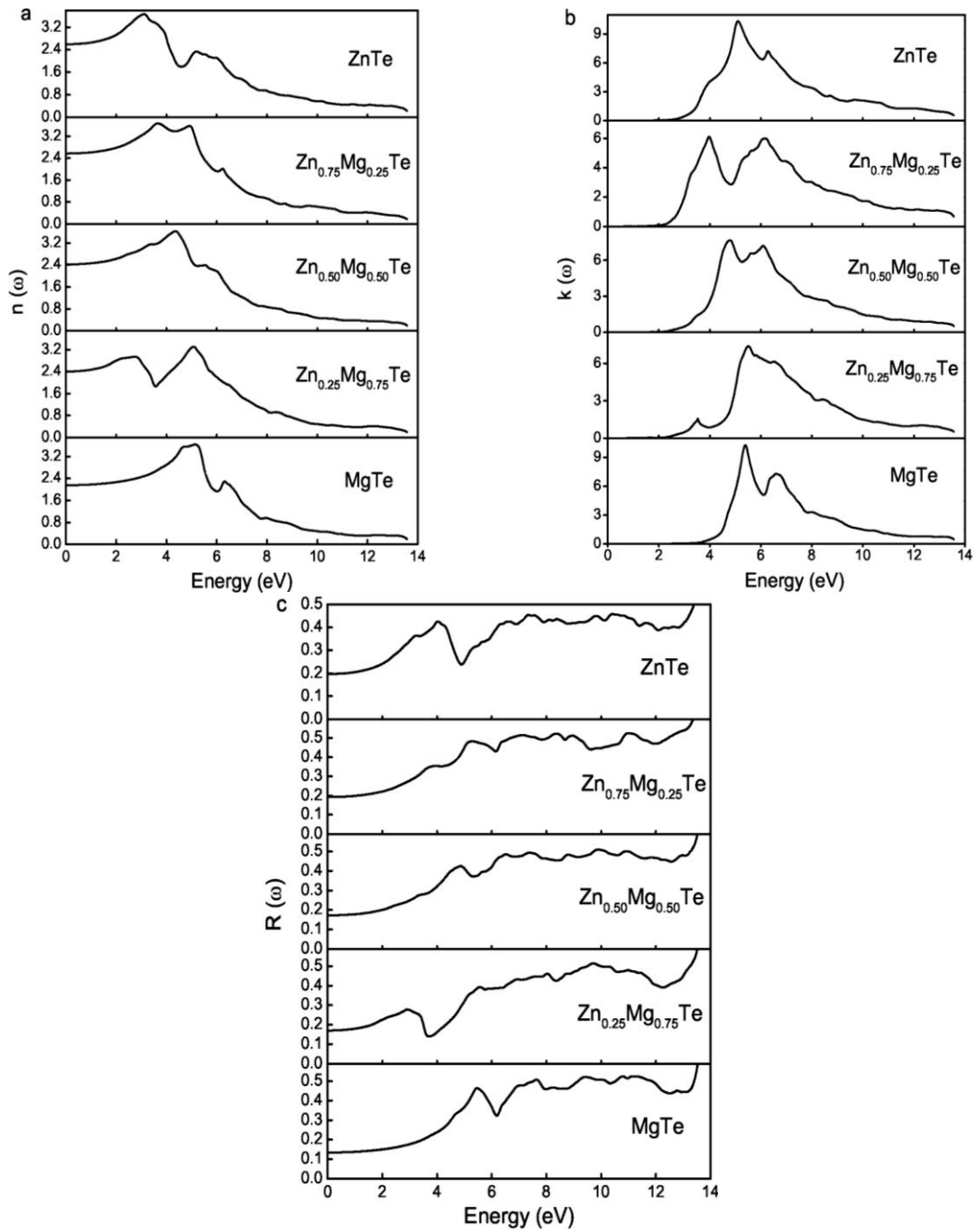


Fig. 6. Calculated (a) refractive index $n(\omega)$, (b) extinction coefficient $k(\omega)$ and (c) reflectivity coefficient $R(\omega)$ of $Zn_{1-x}Mg_xTe$ corresponding to different values of composition x .

Table 3. Calculated optical parameters for $Zn_{1-x}Mg_xTe$ at different Mg concentrations of x .

Composition	Calculated values				Other results	
	$\varepsilon_1(0)$	$R(0)$	$n(0)$	$\varepsilon_2(\omega)$	$\varepsilon_1(0)$	$n(0)$
0.00	6.59	0.19	2.64	2.10	7.04 ^[26]	2.72 ^[41]
0.25	6.38	0.18	2.56	2.17		
0.50	5.95	0.17	2.43	2.35		
0.75	5.42	0.16	2.39	2.41		
1.00	4.91	0.14	2.25	3.56	6.09 ^[28] , 4.70 ^[41]	2.17 ^[41]

4. Conclusion

In this work, we have studied ZnTe and MgTe compounds and their ternary $Zn_{1-x}Mg_xTe$ alloys in zinc blende phase for the calculations of electronic band structures, DOS, charge density, elastic constants and optical properties within the framework of FP-LAPW+lo method using DFT. For calculating electronic band structures, WC, PBEsol, and PBE GGA were used for comparison with mBJ. It was found that mBJ calculate properties were in good agreement with experimental results. The achieved structural properties are in suitable agreement with other theoretical and experimental results for the binary compounds, which supports our calculations for $Zn_{1-x}Mg_xTe$ ternary alloys. The band structures show that $Zn_{1-x}Mg_xTe$ has direct band gaps, which increase with increasing concentration of Mg. Total and partial DOS have been studied in terms of involvement from dissimilar orbitals of the basic atoms. The DOS calculations show that the Zn-3d and Te-5s states dominate the lower part of the valence band and small contribution of Te-5p and Mg-3s states exist at the upper part of the valence band. The elastic constants fulfill the mechanical stability circumstances for all composition of x . Our calculated results for all properties are in accordance quite well with available theoretical and experimental data. The investigated results predict the optical behavior of the $Zn_{1-x}Mg_xTe$ alloys with increasing concentration of Mg.

Acknowledgment

Authors are thankful to the Computational Condensed Matter Physics Laboratory, in Physics Department of National University Singapore (NUS), for providing the computational facilities necessary to carry out this work. We are also thankful to the Higher Education Commission (HEC) of Pakistan for their financial support.

References

- [1] X. Liu, J.K. Furdyna, *J. Appl. Phys.* **95**, 7754 (2004).
- [2] R. Krause-Rehberg, H.S. Leipner, T. Abgarjan, A. Polity, *Appl. Phys. A* **66**, 599 (1998).
- [3] L. Hannachi, N. Bouarissa, *Superlatt. Microstruct.* **44**, 794 (2008).
- [4] F. Benkabou, H. Aourag, M. Certier, T. Kobayasi, *Physica B* **336**, 275 (2003).
- [5] J. M. Gaines, R. R. Drenten, K. W. Haberern, T. Marshall, P. Mensz, J. Petruzzello, *Appl. Phys. Lett.* **62**, 2462 (1993).
- [6] T. Tanaka, Y. Kume, M. Nishio, Q. Guo, H. Ogawa, A. Yoshida, *Jpn. J. Appl. Phys.* **42**, L362 (2003).
- [7] K. Saito, K. Kinoshita, T. Tanaka, M. Nishio, Q. Guo, H. Ogawa, *Phys. Stat. Sol. (c)* **3**, 812 (2006).
- [8] J.J. Polit, E.M. Sheregii, E. Burattini, A. Marcelli, M. Cestelli Guidi, P. Calvani, A. Nucara, M. Piccinini, A. Kisiel, J. Konior, E. Sciesińska, J. Sciesiński, A. Mycielski, *J. Alloys Compd.* **371**, 172 (2004).
- [9] E. Janik, E. Dynowska, P. Dłużewski, S. Kret, A. Presz, W. Zaleszczyk, W. Szuszkiewicz, J.F. Morhange, A. Petrouchik, S. Maćkowski, T. Wojtowicz, *Nanotechnology* **19**, 365606 (2008).
- [10] F. Tran, P. Blaha, *Phys. Rev. Lett.* **102**, 226401 (2009).
- [11] S.D. Guo, B.G. Liu, *Europhys. Lett.* **93**, 47006 (2011).
- [12] F. Tran, P. Blaha, K. Schwarz, *J. Phys.: Condens. Matter* **19**, 196208 (2007).
- [13] Z. Charifi, F. El Haj Hassan, H. Baaziz, S. Khosravizadeh, S.J. Hashemifar, H. Akbarzadeh, *J. Phys.: Condens. Matter* **17**, 7077 (2005).
- [14] A. Zunger, S.H. Wei, L.G. Ferreira, J.E. Bernard, *Phys. Rev. Lett.* **65**, 353 (1990).
- [15] W. Kohn, L. J. Sham, *Phys. Rev.* **140**, A1133 (1965).
- [16] P. Blaha et al., WIEN2k, An Augmented Plane Wave Plus Local Orbital Program for Calculating the Crystal Properties, ed. K. Schwarz (Vienna University of Technology, Austria, 2001).
- [17] C. Ambrosch-Draxl, J. O. Sofo, *Comput. Phys. Commun.* **175**, 1 (2006).
- [18] Z. Wu, R.E. Cohen, *Phys. Rev. B* **73**, 235116 (2006).
- [19] S.J. Chung, E.K. Suh, Y.K. Jun, *J. Korean Phys. Soc.* **46**, 963 (2005).
- [20] B. Amin, I. Ahmad, M. Maqbool, S. Goumri-Said, R. Ahmad, *J. Appl. Phys.* **109**, 023109 (2011).
- [21] A. J. Franz, F. C. Peiris, X. Liu, U. Bindley, J. K. Furdyna, *Phys. Stat. Sol. (b)* **241**, 507 (2004).
- [22] B. Jobst, D. Hommel, U. Lunz, T. Gerhard, G. Landwehr, *Appl. Phys. Lett.* **69**, 97 (1996).
- [23] A. Hossain, V. Yakimovich, A.E. Bolotnikov, K. Bolton, G.S. Camarda, Y. Cui, J. Franc, R. Gul, K.H. Kim, H. Pittman, G. Yang, R. Herpst, R.B. James, *J. Cryst. Growth* **379**, 34 (2013).
- [24] X. Liu, J. K. Furdyna, *J. Appl. Phys.* **95**, 7754 (2004).
- [25] H. Okuyama, Y. Kishita, A. Ishibashi, *Phys. Rev. B* **57**, 2257 (1998).
- [26] L. Hannachi, N. Bouarissa, *Physica B* **404**, 3650 (2009).
- [27] X. Mathew, J. Drayton, V. Parikh, N. R. Mathews, X. Liu, A. D. Compaan, *Semicond. Sci. Technol.* **24**, 015012 (2009).
- [28] A. Sajid, A. Afaq, G. Murtaza, *Chin. J. Phys.* **51**, 316 (2013).
- [29] I. Khan, A. Afaq, H.A. Rahnamaye Aliabad, I. Ahmad, *Comp. Mater. Sci.* **61**, 278 (2012).
- [30] G. Gökoğlu, *J. Phys. Chem. Solids* **71**, 1388 (2010).
- [31] M. Levinshstein, S. Rumyantsev, M. Shur, *Handbook Series on Semiconductor Parameters* (Singapore: World Scientific) 1999.
- [32] M. Romčević, N. Romčević, *J. Alloys Comp.* **416**, 64 (2006).
- [33] S. Mnasri, S. Abdi-Ben Nasrallah, N. Sfina, N. Bouarissa, M. Said, *Semicond. Sci. Technol.* **24**, 095008 (2009).

- [34] R. Khenata, A. Bouhemadou, M. Sahnoun, A. H. Reshak, H. Baltache, M. Rabah, *Comp. Mater. Sci.* **38**, 29 (2006).
- [35] B.H. Lee, *J. Appl. Phys.* **41**, 2988 (1970).
- [36] F. Drief, A. Tadjer, D. Mesri, H. Aourag, *Catal. Today* **89**, 343 (2004).
- [37] J.M. Hu, S.P. Huang, Z. Xie, H. Hu, W.D. Cheng, *J. Phys.: Condens. Matter* **19**, 496215 (2007).
- [38] G. Surucu, K. Colakoglu, E. Deligoz, Y. Ciftci, N. Korozlu, *J. Mater. Sci.* **46**, 1007 (2011).
- [39] R. Ali, S. Mohammad, H. Ullah, S.A. Khan, H. Uddin, M. Khan, N.U. Khan, *Physica* **410**, 93 (2013).
- [40] I. Khan, I. Ahmad, H.A. Rahnamaye Aliabad, S. Jalali Asadabadi, Z. Ali, M. Maqbool, *Comput. Mater. Sci.* **77**, 145 (2013).
- [41] L. Guo, G. Hu, W.J. Feng, S.T. Zhang, *Acta Phys. Chim. Sin.* **29**, 929 (2013).

*Corresponding author: rapakistana@yahoo.com